No-reference image quality assessment based on phase congruency and spectral entropies

Maozheng Zhao, Qin Tu, Yanping Lu, Yongyu Chang, Bo Yang, Aidong men

School of Information and Communication Engineering,Beijing University of Posts and Telecommunications
Beijing, 100876, China
{*maozhengzhao, tuqin, luyanping, yychang, boyang, menad*}*@bupt.edu.cn*

***Abstract*—We develop an efficient general-purpose blind/no-reference image quality assessment (IQA) algorithm that utilizes curvelet domain features of phase congruency values and local spectral entropy values in distorted images. A 2-stage framework of distortion classification followed by quality assessment is used for mapping feature vectors to prediction scores. We utilize a support vector machine (SVM) to train an image distortion and quality prediction model. The resulting algorithm which we name Phase Congruency and Spectral Entropy based Quality (PCSEQ) index is capable of assessing the quality of distorted images across multiple distortion categories. We explain the advantages of phase congruency features and spectral entropy features. We also thoroughly test the algorithm on the LIVE IQA databse and find that PCSEQ correlates well with human judgments of quality. It is superior to the full-reference (FR) IQA algorithm SSIM and several top-performance no-reference (NR) IQA methods such as DIIVINE and SSEQ. We also tested PCSEQ on the TID2008 database to ascertain whether it has performance that is database independent.**

***Index terms*— phase congruency, spectral entropy, no-reference image quality assessment (NR IQA), support vector machine (SVM)**

I. INTRODUCTION

Objective image quality assessment (IQA) aims to build computational models that can evaluate image quality consistently with human perception. With the rapid proliferation of digital imaging and communication technologies, IQA has been becoming an important issue in numerous applications, such as image acquisition, transmission, compression, restoration, and enhancement. Since subjective IQA methods cannot be readily and routinely used in real-time and automated systems, developing objective IQA metrics that can automatically and robustly measure an image's quality becomes necessary. IQA approaches can be classified into three categories based on the availability of nondistorted reference images: full-reference IQA (FR-IQA), reduced-reference IQA (RR-IQA), and no-reference IQA (NR-IQA).

Since the undistorted images are often not available in most cases, NR IQA becomes the only practical method that can be embedded into IQA application systems. For simplicity, most early NR-IQA algorithms assume that the image under consideration is affected by specific types of distortion, such as JP2K in [1] and JPEG in [2]. Generally, these approaches extract distortion-specific features that relate to the loss of visual quality. But their application fields are often limited since they have to know the distortion types in advance.

In contrast, the goal of general-purpose nondistortion-specific (NDS) NR-IQA approaches is to predict an image's quality without any prior knowledge of the distortion type. Most general-purpose quality assessment methods proposed are based on training and learning. Moorthy and Bovik proposed a two step framework for NR IQA which first classifies the distortion type of the distorted image and then implies distortion-specific quality assessment to implement a blind IQA method named BIQI which utilizing several Natural Scene Statistics (NSS) fetures [3]. They later developed DIIVINE index which also based on the two-step framework, it extracts NSS features in the wavelet domain and achieves excellent performance [4]. Saad et al. proposed BLIINDS-II which uses NSS features in the block DCT domain using a fast single-stage framework [5]. BRISQUE extracts features from the spatial domain which results in particularly low time complexity and it achieves superior predictive performance. SSEQ proposed by L.Liu et al. is based on the 2-stage framework, it extracts NSS features in the curvelet domain and achieves very good performance [6].

We also proposed such a curvelet quality assessment method based on 2-stage training framework. Our idea is inspired by the success of SSEQ. Although SSEQ has already achieved excellent performance, we found that its spatial features, which include the mean values and skew values of histograms of block-based spatial entropies for 3 scales of an image, correlate poorly with human perception and achieve poor predictive accuracy when only applying them to the 2-stage framework. In our work, we found that the performance of mean values and skew values of phase congruency (PC) histogram of an image is much better than the spatial features used in SSEQ and is approximate to the spectral features in SSEQ. Hence, we utilize curvelet features (mean values and skew values) extracted from PC histograms and spectral entropy histograms to the 2-stage training framework proposed in [3] and [4] resulting in a novel NR IQA algorithm named Phase Congruency and Spectral Entropy based Quality (PCSEQ) index. Actually, PC has already been applied for IQA in the literature such as [7] and [8], but to the best of our knowledge, it is the first time to use the curvelet domain features of PC to NR IQA. We thoroughly evaluate PCSEQ on LIVE IQA database and prove that PCSEQ performs significantly better than several top-performing NR IQA methods such as SSEQ [6], DIIVINE [4] and FR IQA algorithm SSIM [9].

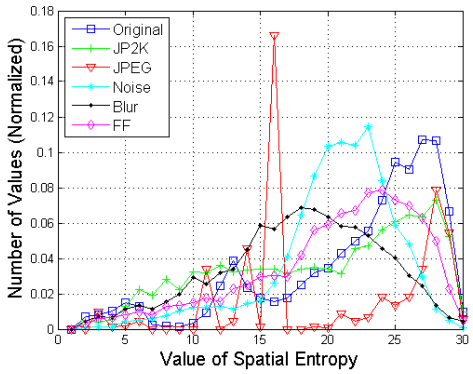

Fig. 1. Histograms of spatial entropies for different types of distortion. The 6 curves correspond to an undistorted image and its distorted counterparts. "Original" (DMOS=0), "JP2K" (DMOS=67.6968), "JPEG" (DMOS=70.5024), "Noise" (DMOS=55.0675), "Blur" (DMOS=68.0166), "FF" (DMOS=64.7162).

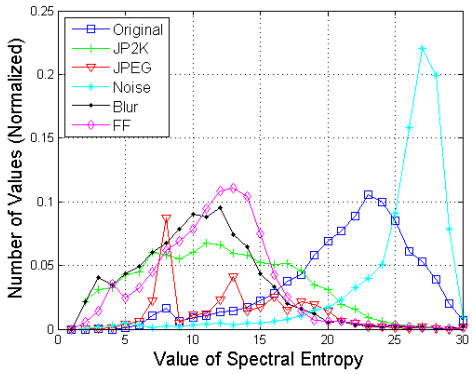

Fig. 2. Histograms of spectral entropies for different types of distortion. The 6 curves correspond to an undistorted image and its distorted counterparts. The images here are the same with those in Fig. 1.

II. Spatial and spectral entropies based NR IQA

SSEQ [6] proposed by L.Liu et al. is established based on the fact that the shapes of spatial entropy and spectral entropy histograms will change regularly under different distortion types and extents. The process of computing spatial and spectral entropies are as follows.

The spatial entropy is

$$E = -\sum_{x} p(x)\log_2 p(x), \tag{1}$$

where x are the pixel values within a block, with empirical probability density $p(x)$.

The spectral entropy is

$$F = -\sum_{i}\sum_{j} P(i,j)\log_2 P(i,j), \tag{2}$$

where $P(i,j)$ is the spectral probability of normalized DCT coefficients.

$$P(i,j) = \frac{C(i,j)^2}{\sum_i \sum_j C(i,j)^2}, \tag{3}$$

where $1 < i \leq 8, 1 < j \leq 8$ (DC is excluded).

The histograms of spatial entropies of one image and its five distortion counter parts are shown in Fig. 1. The mean values and skew values of the undistorted image's histogram will change with different distortion types and extents. The histograms of spectral entropy values of one image in Fig. 2 show the same pattern. The mean values and the skew values of spatial and spectral entropy histograms have the capability of capturing the distortion types and extents of natural images.

Main steps of SSEQ are as follows: First, the input image is down sampled twice to get its 3 scales. Second, the response of each scale is divided into 8×8 blocks on which spatial and spectral entropies are computed. Third, the mean values and skew values of spatial and spectral entropy histograms are computed for each scale. Then, the 12 dimensional feature vector extracted is applied to the 2-stage framework for NR IQA in [3] and [4] to get the predictive score.

III. Phase congruency and spectral entropies based NR IQA

A. Phase congruency features

The physiological and psychophysical evidences had proved that visually discernable features coincide with points where the Fourier waves have congruent phases at different frequencies [10], [11], i.e., at points of high PC values. Besides, PC also have the characteristic of contrast invariance. Thus, the PC theory provides a simple but biologically plausible model of how mammalian visual systems detect and identify features in an image.

In this paper, we adopt the method of computing PC developed by Kovesi [11], which is widely used in literature. We adopt logarithmic Gabor filters [12] for wavelet transform and adopt Gaussian function as the spreading function for the log-Gabor filters to extend to 2D ones. The 2-D log-Gabor filters extended by Gaussian function have the following transfer function:

$$G_2(\omega,\theta_j) = \exp\left(-\frac{\left(\log(\frac{\omega}{\omega_0})\right)^2}{2\sigma_r^2}\right)\cdot\exp\left(-\frac{(\theta-\theta_j)^2}{2\sigma_\theta^2}\right), \tag{4}$$

where where ω_0 is the filter's center frequency, and σ_r controls the filters bandwidth, $\theta_j = j\pi/J$, $j = \{0,1,...,J-1\}$ is the orientation angle of the filter, J is the number of orientations, and σ_θ determines the filter's angular bandwidth.

Denoted by M^e_{n,θ_j} and M^o_{n,θ_j} the even- and odd-symmetric filters of the 2-D log-Gabor filters on scale n and orientation θ_j, and they form a quadrature pair. By modulating ω_0 and θ_j and convolving G_2 with an image, we get a set of responses at each point x as $\lfloor e_{n,\theta_j}(x), o_{n,\theta_j}(x)\rfloor$, where $e_{n,\theta_j}(x)$ and $o_{n,\theta_j}(x)$ are responses of the quadrature pair on scale n and orientation θ_j at location x. The local amplitude on scale n and orientation θ_j is $A_{n,\theta_j}(x) = \sqrt{e_{n,\theta_j}(x)^2 + o_{n,\theta_j}(x)^2}$,

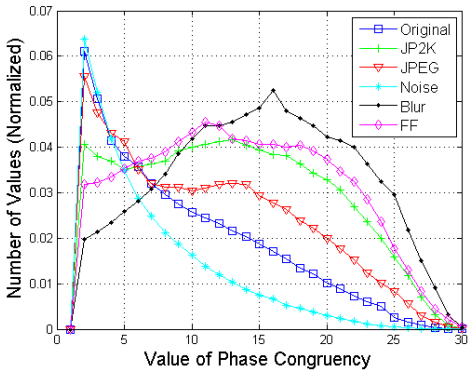

Fig. 3. Histograms of phase congruency values for different types of distortion. The 6 curves correstpond to an undistorted image and its distorted counterparts. The images here are the same with those in Fig. 1.

and the local energy along orientation θ_j is $E_{\theta_j}(x) = \sqrt{F_{\theta_j}(x)^2 + H_{\theta_j}(x)^2}$, where $F_{\theta_j}(x) = \sum_n e_{n,\theta_j}(x)$ and $H_{\theta_j}(x) = \sum_n o_{n,\theta_j}(x)$. The 2-D PC at x is defined as follows:

$$PC(x) = \frac{\sum_j E_{\theta_j}(x)}{\lambda + \sum_n \sum_j A_{n,\theta_j}(x)} \quad (5)$$

where λ is a small positive constant to keep the fraction stable when all the Fourier amplitudes are very small. $PC(x)$ is a real number within $0-1$.

B. Phase congruency and spectral entropies based index

The histogram of PC values of one image and its distortion counterparts are shown in Fig. 3. The histograms of PC values are more smooth and more regular than that of the spatial entropies in Fig. 1 and also change with different distortion types and extents. From the experiments in section IV, we can prove that the performance of mean values and skew values of PC histogram of an image is much better than the spatial features used in SSEQ and is approximate to the spectral features in SSEQ.

Hence, we substitute PC features for spatial entropy features in SSEQ. Utilizing curvelet features (mean values and skew values) extracted from PC histograms and spectral entropy histograms to the 2-stage training frame work proposed in [3] and [4] results in a novel NR IQA algorithm named Phase Congruency and Spectral Entropy based Quality (PCSEQ) index. PCSEQ can be divided into four steps:

1) Down sampling. The incoming distorted image is down sampled with a factor of 2. In this method, each assessed image is decomposed into 3 scales since we found that increasing or decreasing the number of scales did not contribute much.

2) Feature computing. Spectral entropy values F on 8×8 blocks and PC values PC on pixels are computed for each scale. The definition of spectral entropy used here is the same as equation (2) and (3).

3) Feature pooling. By sorting PC values and spectral entropies in ascending order, the ordered sets $PC = (pc_1, pc_2, ..., pc_m)$ and $F = (fe_1, fe_2, ..., fe_n)$ are yielded. Here pc_i and fe_j are PC values and local spectral entropies, m and n are the number of pixels and blocks respectively within each scale. Then percentile pooling is implied to F and PC since the histograms are more stable at the central segment. Extracting the central 60% elements from F and PC yields $Fp = (fe_{\lfloor 0.2n \rfloor}, fe_{\lfloor 0.2n \rfloor+1}, ..., fe_{\lfloor 0.8n \rfloor})$ and $PCp = (pc_{\lfloor 0.2m \rfloor}, pc_{\lfloor 0.2m \rfloor+1}, ..., pc_{\lfloor 0.8m \rfloor})$. The mean values of PCp and Fp and the skew values of PC and F make up the final features of each scale:

$$f = (mean(PCp), skew(PC), mean(Fp), skew(F)). \quad (6)$$

4) Prediction. Each incoming image is decomposed into 3 scales and 4 features are extracted from each scale. So each distorted image has a feature vector of $3 \times 4 = 12$ dimensions. A two-stage framework for NR IQA is utilized to the feature vector to get the final image quality score.

The two-stage framework used here is the same as that in [3], [4]. A probabilistic classifier is trained to compute the probability of occurrence of each distortion type in an image, and then regression functions are trained on each distortion type against human scores. The two models yield a distortion probability vector and a distortion specific quality vector respectively for each incoming image. Then the dot product of the two vectors results in the final predictive score.

We use a support vector machine (SVM) for classification and SVR for regression [13], [14]. The SVM and SVR used here are implemented by the LIBSVM package [15], the radial basis function (RBF) is used in both implementation.

IV. EXPERIMENTS AND RESULTS

We test the performance of PCSEQ on the LIVE database [16], which contains 29 reference images each with five different types of distortions - JPEG2k (JP2K), JPEG, white Gaussian noise (Noise), Gaussian blurring (Blur) and fast fading channel distortion (FF), at 5 to 6 different levels. The differential mean opinion score (DMOS) of distorted images are provided.

The results reported in this section of the 2-stage framework are obtained by 1000 train-test iterations with randomly selected 80% of the reference images and their distorted counterparts as training set and the remaining 20% of the reference images and their distorted counterparts as testing set. We use the realigned DMOS scores [17] for the LIVE database.

We evaluate our system performance by Spearman Rank Order Correlation Coefficient (SROCC) and Linear Correlation Coefficient (LCC). SROCC measure the prediction monotonicity of an IQA metric which only operate on the rank of the data points. LCC can be considered as a measure of prediction accuracy of a model. Before computing LCC, the algorithm scores were passed through a logistic nonlinearity as described in [17].

A. Feature prediction power Comparison

In order to study the prediction power of each feature groups and prove the effectiveness of PC features, we conducted two validation experiments on different features. The specific meaning of each feature used here are tabulated in Table I.

TABLE I
FEATURES FOR COMPARATION.

Feature vector	Feature description
f1-f3	Means of spectral entropy values for 1-3 scales
f4-f6	Skews of spectral entropy values for 1-3 scales
f7-f9	Means of spatial entropy values for 1-3 scales
f10-f12	Skews of spatial entropy values for 1-3 scales
f13-f15	Means of phase congruency values for 1-3 scales
f16-f18	Skews of phase congruency values for 1-3 scales

We first study each feature's correlation with DMOS on LIVE for the first scale, namely the original scale, the correlation on other two scales comply with the similar regularity. We directly compute the SROCC between these feature values and the DMOS, the results are shown in Table II.

TABLE II
SROCC BETWEEN FEATURE VALUES OF FIRST SCALE AND DMOS.

	JP2K	JPEG	Noise	Blur	FF
f1	-0.9052	-0.9432	0.9462	-0.9408	-0.8323
f4	0.8405	0.8429	-0.3768	0.8405	0.7671
f7	-0.1081	-0.6914	0.6392	-0.4832	-0.3234
f10	0.0630	0.6129	-0.1453	0.3138	0.1807
f13	0.8638	0.7190	-0.9510	0.9183	0.8104
f16	-0.8720	-0.7061	0.7970	-0.9132	-0.8244

From Table II, we can observe that the mean values of spectral entropy histograms on the first scale (f_1) correlate best with human perception on five distortion types comparing with two other mean values (f_7 and f_{13}), the mean values of PC histograms (f_{13}) correlate much better than that of spatial histograms (f_7). As for skew values, the skew values of PC histograms (f_{16}) correlate best with human perception except on "JPEG" while the SROCC of skew values of spatial histograms (f_{10}) are lowest on each distortion type. We can conclude that the PC features (f_{13} and f_{16}) correlate with human perception much better than spatial entropy features (f_7 and f_{10}).

In order to further study the predictive power of each feature groups when implied them to the 2-stage framework, we evaluate each feature group on each distortion category and across all distortion categories. The median experimental results of these feature subsets over 1000 iterations in terms of SROCC and LCC are tabulated in Table III.

We can observe from Table III that the spectral entropy features ($f_1 - f_6$) performs best while the spatial entropy features ($f_7 - f_{12}$) perform worst and the PC features ($f_{13} - f_{18}$) perform much better than the spatial entropy features ($f_7 - f_{12}$), especially on "JP2K" and "FF" distortion types. We have similar observations on Fig. 2 and Fig. 3. The curves of "JP2K" and "FF" for PC values are quite different from that of "Original", while they are more similar with that of "Original" in spatial entropy histograms.

B. Comparison with other IQA approaches

We compared performance of PCSEQ with three FR approaches (PSNR [18], SSIM [9] and VIF [19]) and other three NR IQA models (SSEQ [6], DIIVINE [4], and BRISQUE [20]). Since FR methods do not need training, we also perform a random 20% test set selection for 1000 times to get median performance indices in order to make a fair comparison. And we only test the methods on the distorted images. For the NR approaches, the same random $80 - 20\%$ train test trails was conducted for 1000 times and the median performance indices was reported. Higher SROCC and LCC mean better quality prediction performance. The results are tabulated in Table IV. The SROCC values of PCSEQ are higher than that of SSEQ on each distortion type and across all distortion types. We can also observe that PCSEQ delivers higher SROCC and LCC values than FR-IQA PSNR, SSIM and NR-IQA DIIVINE across all distortion types (the columns marked by "ALL") but PCSEQ delivers lower SROCC and LCC values than BRISQUE across all distortion types.

C. Classification accuracy

We also report the classification accuracies of PCSEQ and SSEQ for completeness. The median classification accuracies of 1000 train-test trails are shown in Table V. We can observe that the over all classification accuracy of PCSEQ is slightly higher than that of SSEQ.

TABLE V
MEDIAN CLASSIFICATION ACCURACY ACROSS 1000 TRAIN-TEST TRIALS.

	JP2K	JPEG	Noise	Blur	FF	ALL
SSEQ	66.67	86.84	100.00	66.67	46.67	73.13
PCSEQ	71.43	93.12	100.00	63.33	43.33	74.53

D. Database independence

In order to demonstrate the degree of database independence of PCSEQ, we trained it on the entire LIVE database and applied it to the TID2008 database. The TID database consists of 25 reference images and 1700 distorted images over 17 distortion categories [21]. Of the 25 reference images only 24 are natural images, we test PCSEQ on the 24 natural reference images only on distortions that are shared by the two databases: JP2K, JPEG, Gaussian noise (Noise), and Gaussian blur (Blur). The results are shown in Table VI. Compared with PSNR, SSIM, BRISQUE and SSEQ, the correlation with DMOS of PCSEQ remained consistently competitive.

TABLE VI
SROCC OBTAINED BY TRAINING ON THE LIVE IQA DATABASE AND TESTING ON THE TID2008 DATABSE.

	JP2K	JPEG	Noise	Blur	ALL
PSNR	0.7848	0.8585	0.9147	0.8914	0.7527
SSIM(SS)	0.9603	0.9354	0.8168	0.9598	0.9016
BRISQUE	0.9037	0.9102	0.8227	0.8742	0.8977
SSEQ	0.9112	0.8629	0.7986	0.8531	0.8501
PCSEQ	0.8618	0.9065	0.7765	0.8589	0.8840

TABLE III
MEDIAN SROCC AND LCC ACROSS 1000 TRAIN-TEST TRIALS FOR EACH FEATURE GROUP.

	SROCC						LCC					
	JP2K	JPEG	Noise	Blur	FF	ALL	JP2K	JPEG	Noise	Blur	FF	ALL
f1-f6	0.9157	0.9268	0.9301	0.9217	0.8449	0.8933	0.9224	0.9302	0.9406	0.9298	0.8703	0.9004
f7-f12	0.6404	0.8725	0.9146	0.7448	0.6040	0.7568	0.6584	0.8919	0.9202	0.7720	0.6788	0.7689
f13-f18	0.8458	0.8630	0.9528	0.8892	0.8258	0.7826	0.8338	0.8810	0.9662	0.8852	0.8519	0.7880

TABLE IV
MEDIAN SROCC AND LCC ACROSS 1000 TRAIN-TEST TRIALS ON THE LIVE IQA DATABASE.

	SROCC						LCC					
	JP2K	JPEG	Noise	Blur	FF	ALL	JP2K	JPEG	Noise	Blur	FF	ALL
PSNR	0.8692	0.8872	0.9417	0.7593	0.8741	0.8665	0.8638	0.8833	0.8967	0.7855	0.8663	0.8602
SSIM(SS)	0.9401	0.9492	0.9644	0.9097	0.9413	0.9143	0.9535	0.9605	0.9826	0.9067	0.9586	0.9074
VIF	0.9683	0.9819	0.9844	0.9720	0.9622	0.9629	0.9809	0.9885	0.9897	0.9771	0.9716	0.9600
DIIVINE	0.9031	0.9037	0.9831	0.9288	0.8412	0.9084	0.9075	0.9115	0.9770	0.9244	0.8589	0.9035
BRISQUE	0.9095	0.9645	0.9778	0.9511	0.8759	0.9363	0.9120	0.9733	0.9848	0.9457	0.9013	0.9385
SSEQ	0.8971	0.9427	0.9640	0.9155	0.8536	0.9121	0.9026	0.9608	0.9695	0.9289	0.8745	0.9177
PCSEQ	0.9059	0.9453	0.9689	0.9333	0.8572	0.9226	0.9101	0.9516	0.9750	0.9397	0.8808	0.9245

V. CONCLUSION

We proposed an efficient general-purpose NR IQA model called Phase Congruency and Spectral Entropy based Quality (PCSEQ) index, which utilizes curvelet domain NSS features. We elaborate the algorithm and the statistical features extracted and demonstrate how each of these features correlate with human perception. We demonstrate that PCSEQ delivers quality prediction performance that is competitive with top-performing NR and FR models and found that PCSEQ performance is also independent of database content. However, PCSEQ can not avoid the common deficiency of training based NR IQA that it can only reach great performance on the distortion types which it has been trained for. We will continue our future work on NR IQA models which do not need training.

ACKNOWLEDGEMENT

This work is supported by the National Science Foundation of China (61271190).

REFERENCES

[1] ZM Parvez Sazzad, Yoshikazu Kawayoke, and Yuukou Horita, "No reference image quality assessment for jpeg2000 based on spatial features," *Signal Processing: Image Communication*, vol. 23, no. 4, pp. 257–268, 2008.

[2] Zhou Wang, Alan C Bovik, and BL Evan, "Blind measurement of blocking artifacts in images," in *Image Processing, 2000. Proceedings. 2000 International Conference on*. Ieee, 2000, vol. 3, pp. 981–984.

[3] Anush K Moorthy and Alan C Bovik, "A two-step framework for constructing blind image quality indices," *Signal Processing Letters, IEEE*, vol. 17, no. 5, pp. 513–516, 2010.

[4] Anush Krishna Moorthy and Alan Conrad Bovik, "Blind image quality assessment: From natural scene statistics to perceptual quality," *Image Processing, IEEE Transactions on*, vol. 20, no. 12, pp. 3350–3364, 2011.

[5] Michele A Saad, Alan C Bovik, and Christophe Charrier, "Blind image quality assessment: A natural scene statistics approach in the dct domain," *Image Processing, IEEE Transactions on*, vol. 21, no. 8, pp. 3339–3352, 2012.

[6] Lixiong Liu, Bao Liu, Hua Huang, and Alan Conrad Bovik, "No-reference image quality assessment based on spatial and spectral entropies," *Signal Processing: Image Communication*, vol. 29, no. 8, pp. 856–863, 2014.

[7] Rania Hassen, Zhou Wang, and Magdy Salama, "No-reference image sharpness assessment based on local phase coherence measurement," in *Acoustics Speech and Signal Processing (ICASSP), 2010 IEEE International Conference on*. IEEE, 2010, pp. 2434–2437.

[8] Lin Zhang, D Zhang, and Xuanqin Mou, "Fsim: a feature similarity index for image quality assessment," *Image Processing, IEEE Transactions on*, vol. 20, no. 8, pp. 2378–2386, 2011.

[9] Zhou Wang, Alan C Bovik, Hamid R Sheikh, and Eero P Simoncelli, "Image quality assessment: from error visibility to structural similarity," *Image Processing, IEEE Transactions on*, vol. 13, no. 4, pp. 600–612, 2004.

[10] M Concetta Morrone and DC Burr, "Feature detection in human vision: A phase-dependent energy model," *Proceedings of the Royal Society of London. Series B, biological sciences*, pp. 221–245, 1988.

[11] Peter Kovesi, "Image features from phase congruency," *Videre: Journal of computer vision research*, vol. 1, no. 3, pp. 1–26, 1999.

[12] David J Field, "Relations between the statistics of natural images and the response properties of cortical cells," *JOSA A*, vol. 4, no. 12, pp. 2379–2394, 1987.

[13] Bernhard Schölkopf, Alex J Smola, Robert C Williamson, and Peter L Bartlett, "New support vector algorithms," *Neural computation*, vol. 12, no. 5, pp. 1207–1245, 2000.

[14] Christopher JC Burges, "A tutorial on support vector machines for pattern recognition," *Data mining and knowledge discovery*, vol. 2, no. 2, pp. 121–167, 1998.

[15] Chih-Chung Chang and Chih-Jen Lin, "LIBSVM: A library for support vector machines," *ACM Transactions on Intelligent Systems and Technology*, vol. 2, pp. 27:1–27:27, 2011, Software available at http://www.csie.ntu.edu.tw/∼cjlin/libsvm.

[16] H.R. Sheikh, Z. Wang, L. Cormack, and A.C. Bovik, "Live image quality assessment database release 2," 2006, Available from: http://live.ece.utexas.edu/research/quality.

[17] Hamid R Sheikh, Muhammad F Sabir, and Alan C Bovik, "A statistical evaluation of recent full reference image quality assessment algorithms," *Image Processing, IEEE Transactions on*, vol. 15, no. 11, pp. 3440–3451, 2006.

[18] Zhou Wang and Alan C Bovik, "Mean squared error: love it or leave it? a new look at signal fidelity measures," *Signal Processing Magazine, IEEE*, vol. 26, no. 1, pp. 98–117, 2009.

[19] Hamid R Sheikh and Alan C Bovik, "Image information and visual quality," *Image Processing, IEEE Transactions on*, vol. 15, no. 2, pp. 430–444, 2006.

[20] Anish Mittal, Anush Krishna Moorthy, and Alan Conrad Bovik, "No-reference image quality assessment in the spatial domain," *Image Processing, IEEE Transactions on*, vol. 21, no. 12, pp. 4695–4708, 2012.

[21] Nikolay Ponomarenko, Vladimir Lukin, Alexander Zelensky, Karen Egiazarian, M Carli, and F Battisti, "Tid2008-a database for evaluation of full-reference visual quality assessment metrics," *Advances of Modern Radioelectronics*, vol. 10, no. 4, pp. 30–45, 2009.